Acta Pharmacologica Sinica

ARTICLE

Monocarbonyl curcumin analog A2 potently inhibits angiogenesis by inducing ROS-dependent endothelial cell death

Bin Liu[1], Liu-su Cui[2], Bo Zhou[3], Ling-ling Zhang[1], Zhi-hui Liu[1] and Lu Zhang[1]

Excessive and abnormal vessel growth plays a critical role in the pathogenesis of many diseases, such as cancer. Angiogenesis is one of the hallmarks of cancer growth, invasion, and metastasis. Discovery of novel antiangiogenic agents would provide new insights into the mechanisms of angiogenesis, as well as potential drugs for cancer treatment. In the present study, we investigated the antiangiogenic activity of a series of monocarbonyl analogs of curcumin synthesized previously in our lab. We found that curcumin analog A2 displayed the full potential to be developed as a novel antiangiogenic agent. Curcumin analog A2 at and above 20 μM dramatically inhibited the migration and tube formation of human umbilical vein endothelial cells (HUVECs) in vitro, new microvessels sprouting from the rat aortic rings ex vivo and newly formed microvessels in chicken chorioallantoic membranes (CAMs) and Matrigel plus in vivo. We further demonstrated that curcumin analog A2 exerted its antiangiogenic activity mainly through inducing endothelial cell death via elevating NADH/NADPH oxidase-derived ROS. Curcumin analog A2 at the antiangiogenic concentrations also triggered autophagy in HUVECs, but this process is neither a pre-requisite for toxicity, leading to the cell death nor a protective response against the toxicity of curcumin analog A2. In conclusion, we demonstrate for the first time the potent antiangiogenic activity of the monocarbonyl curcumin analog A2, which could serve as a promising potential therapeutic agent for the prevention and treatment angiogenesis-related diseases, such as cancer.

Keywords: monocarbonyl curcumin analog; angiogenesis; apoptosis; autophagy; necroptosis; reactive oxygen species; vascular endothelial cell; bafilomycin A1; wortmannin

Acta Pharmacologica Sinica (2019) 40:1412–1423; https://doi.org/10.1038/s41401-019-0224-x

INTRODUCTION

Angiogenesis is defined as the sprouting of new blood vessels from preexisting ones, and it usually occurs during embryonic development, wound healing, bone remodeling, and organ growth [1]. However, excessive and abnormal vessel growth plays a critical role in the pathogenesis of many diseases, such as cancer [1]. Neoangiogenesis is essential not only for cancer cell growth, as it supplies blood, but also for cancer cell invasion and metastasis, as it enables cells to enter the circulation [2]. Unlike cancer cells, vascular endothelial cells (VECs) within the tumor microenvironment are generally genetically stable and, thus theoretically less likely to develop drug resistance [3]. Nevertheless, we must be aware that serious side effects, such as hypertension, bleeding, gastrointestinal perforation, and other reported problems, have been associated with the use of currently available antiangiogenic agents, limiting their application in clinical settings [4]. In addition, the use of antiangiogenic medications is much more limited than the theoretical therapeutic possibilities existing for angiogenesis. The discovery of more compounds possessing potent antiangiogenic activities has important clinical significance.

Curcumin (diferuloylmethane) is an active ingredient of the spice turmeric, *Curcuma longa*, that exhibits many pharmacological activities, including antioxidant, anti-inflammatory, antidiabetic, antimicrobial, and antitumor activities [5]. Several studies have demonstrated that curcumin inhibits angiogenesis by modulating various cell signaling pathways [5–8]. Despite much evidence of its efficacy and safety as an angiogenesis inhibitor, curcumin has not yet been approved for clinical use due to its poor absorption, rapid metabolism, and elimination in vivo [9]. However, curcumin offers a good lead compound for further structural modification, as several curcumin analogs or derivatives have been found to inhibit angiogenesis [10–12].

A growing number of studies have shown that monocarbonyl analogs of curcumin without the β-diketone moiety exhibit higher stability and safety and better pharmacokinetic profiles and in vitro and in vivo activities than curcumin [12–16]. Previously, we synthesized a collection of monocarbonyl analogs of curcumin in our laboratory [17]. Interestingly, most of these analogs showed stronger antitumor activity than curcumin in human non-small-cell lung cancer A549 cells [17]. In the present study, after screening, we identified curcumin analog A2 (Fig. 1) with a high potential to be developed as an antiangiogenic agent.

[1]College of Bioengineering, Henan University of Technology, Zhengzhou 450001, China; [2]Morphological laboratory, Xinxiang Medical University, Xinxiang 453003, China and [3]State Key Laboratory of Applied Organic Chemistry, Lanzhou University, Lanzhou 730000, China
Correspondence: Lu Zhang (zhanglu@haut.edu.cn)

Received: 27 November 2018 Accepted: 26 February 2019
Published online: 18 April 2019

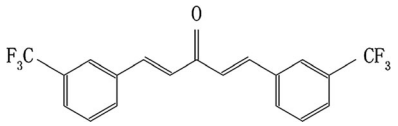

Fig. 1 The chemical structure of curcumin analog A2. The molecular formula of this compound is $C_{19}H_{12}OF_6$, and its molecular weight is 370.2879 g/mol

MATERIALS AND METHODS

Materials and antibodies

The compound curcumin analog A2 was synthesized in our laboratory (purity of at least 99% by high-performance liquid chromatography) and dissolved in dimethyl sulfoxide (DMSO) to make a 0.1 M stock solution, which was stored at −20 °C and diluted with proper medium to various concentrations before use. Fetal bovine serum (FBS; SH30084.03) for human umbilical vein vascular endothelial cell (HUVEC) culture was obtained from HyClone (Logan, Utah, USA). Recombinant human vascular endothelial growth factor (VEGF, PHC9394) was purchased from Gibco (California, USA). MCDB 131 medium (M8537–10 × 1 L), trypsin (T4799-10G), Earle's Balanced Salt Solution (EBSS; E2888), 3-methyladenine (3-MA; V900930), thiazolyl blue tetrazolium bromide (MTT; M2128), Hoechst 33258 (B2883), diphenyleneiodonium chloride (DPI; D2926), and protease inhibitor cocktail (P8340) were purchased from Sigma-Aldrich (St. Louis, Montana, USA). Bafilomycin A_1 (1334) was obtained from Merck (Darmstadt, Germany). Premo™ Autophagy Tandem Sensor RFP-GFP-LC3B Kit (P36239), TRIzol™ (15596026), Opti-MEM™ (31985062), Lipofectamine™ RNAiMAX transfection reagent (13778150), scrambled small-interfering RNA (siRNA; 462001) and MitoSOX™ Red Mitochondrial Superoxide Indicator (M36008) were purchased from Thermo Fisher Scientific (Waltham, Massachusetts, USA). DCFH-DA (S0033), JC-1 (C2006), wortmannin (s1952) and N-acetylcysteine (NAC; S0077) were purchased from Beyotime Biotechnology (Shanghai, China). Annexin V-FITC apoptosis detection kit I (556547) and Matrigel (354234) were purchased from BD Biosciences (Franklin Lakes, New Jersey, USA). Caspase-Glo® 3/7 reagent (G8090) was obtained from Promega (Madison, Wisconsin, USA). Hemoglobin test solution (C021) and LDH kit (A020-1) were purchased from NanJing JianCheng (Nanjing, China). ChamQ Universal SYBR quantitative PCR Master Mix (Q711-02) was obtained from Vazyme Biotechnology (Beijing, China). DMSO (A600163-0500), Tris (A600194-0500), bis-acrylamide (A600025-0250), sodium dodecyl sulfate (SDS; A100227), ammonium persulfate (A600072-0100), paraformaldehyde (E672002-0500) and RevertAid First Strand cDNA Synthesis Kit (B300538-0020) were purchased from Shanghai Sangon Biotech (Shanghai, China). Specific siRNAs against ATG5 (sc-41445) were purchased from Santa Cruz Biotechnology (California, USA). The primary antibody against poly (ADP-ribose) polymerase 1 (PARP1; AP102) was purchased from Beyotime Biotechnology (Shanghai, China). Primary antibodies against microtubule-associated protein 1 light chain 3 beta (MAP1LC3B/LC3B; L7543), Sequestosome 1 (SQSTM1; P0067), glyceraldehyde-3-phosphate dehydrogenase (GAPDH; G9545), mechanistic target of rapamycin kinase (MTOR; T2949), phospho (p)-MTOR (SAB4504476) and BECLIN1 (B6061) were purchased from Sigma-Aldrich (St. Louis, Montana, USA). Primary antibodies against P70S6K (9202s), p-P70S6K (9206s), and ATG5 (D5F5U) were purchased from Cell Signaling Technology (Boston, USA). Secondary IRDye® 800CW goat anti-rabbit (926–32211) and IRDye® 800RD goat anti-mouse (926–32210) antibodies were purchased from Li-Cor Biosciences (Lincoln, Nebraska, USA). The secondary antibody TRITC-conjugated goat anti-rabbit IgG (ZF-0316) was purchased from Beijing ZSGB-BIO (Beijing, China). Nitrocellulose membranes (1620112, 1620115) were obtained from Bio-Rad (California, USA).

Cell culture and treatment

HUVECs were isolated from umbilical cord veins of five healthy donors according to Jaffe et al. [17]. The cells were cultured on gelatin-coated plastic dishes in MCDB 131 medium supplemented with 20% FBS and 70 ng/mL fibroblast growth factor 2 in a humidified incubator at 37 °C with 5% CO_2. HUVECs at no more than passage 8 were used and treated in different ways as follows: (1) the cells were treated with DMSO or various concentrations of curcumin analog A2 in the presence of VEGF (10 ng/mL) for the durations indicated in the Figures; (2) the cells were preincubated with or without various inhibitors and then treated with DMSO or 20 μM curcumin analog A2 in the presence of VEGF (10 ng/mL) for the durations indicated in the figures; or (3) the cells were transfected with scrambled siRNAs or siRNAs against ATG5 for 48 h and then treated with DMSO or 20 μM curcumin analog A2 in the presence of VEGF (10 ng/mL) for the durations indicated in the figures.

Wound healing assay

Endothelial cell migration was evaluated using scratch wound healing assays. Briefly, HUVECs were seeded in 24-well cell culture plates. The cells were cultured with medium containing 1% FBS for 24 h to render them quiescent after they reached confluence. Then, the cells along a straight-line were scraped out using pipette tips and washed twice with media to remove detached cells. Subsequently, HUVECs were treated as described above. Migration was documented using photos captured immediately after scraping and 24 h later. Initial and final wound sizes were measured using AxioVision Rel.4.7 software, and the difference between the two sizes was used to determine migration distance using the following formula: migration distance = (initial wound size – final wound size)/2

Capillary-like tube formation assay

Prechilled 96-well plates were coated with 50 μL growth factor-reduced Matrigel. After Matrigel polymerization for 1 h at 37 °C, HUVECs were seeded in coated plates at 4×10^4 cells per well and treated as described above. The formed endothelial tubes were photographed under an inverted phase-contrast microscope (Nikon, Tokyo, Japan) with a magnification of ×100. The extent of tube formation was assessed by measuring the length of tubes in five random fields from each well using ImageJ (NIH, Bethesda, Maryland, USA).

Aortic ring sprouting assay

Aortic ring sprouting assays were carried out as previously reported [18]. Briefly, thoracic aortas were dissected from 8-week-old Sprague-Dawley rats (purchased from Laboratory Animal Center of Zhengzhou University, Zhengzhou) and cut into 1-mm-thick rings. The aortic rings were placed in Matrigel-coated 96-well plates and sealed in place with an overlay of 40 μL Matrigel. Subsequently, the aortic rings were treated with DMSO, various concentrations of curcumin analog A2, NAC or NAC in combination with curcumin analog A2. On day 7, the sprouting vessels were photographed under an inverted phase-contrast microscope (Nikon, Tokyo, Japan) with a magnification of ×40. The number of vessels sprouting in five randomly chosen fields was counted using a National Institutes of Health (NIH) imaging program. All procedures were performed in accordance with the Guide for the Care and Use of Laboratory Animals published by the US National Institutes of Health (NIH Publication No. 85–23, revised 1996) and approved by the Animal Care Committee of Henan University of Technology.

Chicken chorioallantoic membrane (CAM) assay

CAM assays were carried out according to previously reported methods [18]. Briefly, fertilized chicken eggs were incubated in a humidified incubator at 37 °C for 5 days. On day 6, a small window

was punched on the air sac side of the egg, and a window was created through the egg shell. Then, the CAM was carefully separated from the shell membrane. Sterilized filter paper disks saturated with DMSO, various concentrations of curcumin analog A2, NAC or NAC in combination with curcumin analog A2 were placed on the membrane. The cavity was covered with parafilm, and the chicken eggs were incubated for an additional 2 days. After incubation, CAMs were removed for further analysis. Neovascular zones under the filter paper disks were photographed using a Canon EOS 550D Digital SLR camera. Angiogenesis was quantified by counting the number of branching blood vessels. Assays for each test sample were carried out using 12 eggs.

Matrigel plug assay

Approximately 500 μL Matrigel containing 100 ng/mL VEGF, 100 U heparin and 0 or 20 μM curcumin analog A2 was subcutaneously injected into the dorsal region of 8-week-old C57BL/6 mice purchased from the Department of Laboratory Animal Science, Peking University Health Science Center, China. The injected Matrigel rapidly formed a single, solid gel plug. On day 14, the Matrigel plugs were harvested and photographed using a Canon EOS 550D Digital SLR camera. Neovascularization was assessed by measuring hemoglobin content of the plugs using hemoglobin test solution according to the manufacturer's instructions. All procedures were performed in accordance with the Guide for the Care and Use of Laboratory Animals published by the US National Institutes of Health (NIH Publication No. 85–23, revised 1996) and approved by the Animal Care Committee of Henan University of Technology.

siRNA transfection

HUVECs at 80% confluence were transfected with siRNAs against ATG5 using Lipofectamine™ RNAiMAX transfection reagent. The cells were transfected for 6 h, followed by incubation with fresh MCDB 131 medium for 48 h.

Cell viability assay

Cell viability assays were carried out in real-time using the xCELLigence RTCA S16 System (ACEA Biosciences). Briefly, HUVECs were seeded in E-Plate 16 PET overnight and treated as described above. Changes in the cell index can be used to monitor cell viability. Data were acquired and analyzed using RTCA S16 Software (version 1.0) supplied with the instrument. Furthermore, cell viability was measured using the MTT assay according to our previous study [18].

Annexin V/PI double-staining assay

After treatment, cells were stained using the Annexin V-FITC/PI detection kit following the manufacturer's protocols. Data acquisition and data analysis were carried out using flow cytometry (BD FACSCalibur) and Cell Quest software.

Western blot analysis

After treatment, HUVECs were harvested and lysed in lysis buffer containing 2% SDS, 25 mM Tris-HCl (pH 6.8), 6% glycerol, 1% 2-mercaptoethanol, 2 mM PMSF, 0.02% bromophenol blue and a protease inhibitor cocktail. Equal amounts of total proteins were separated by 12% or 15% SDS-polyacrylamide gel electrophoresis and transferred onto nitrocellulose membranes. Then, the membranes were blocked with 5% (w/v) BSA and 0.05% Tween-20 in phosphate-buffered saline (PBS-T), followed by incubation with different primary antibodies at 4 °C overnight. The membranes were blotted with the corresponding secondary antibodies, and protein bands were scanned using a Li-Cor Odyssey system (Li-Cor Biosciences). The images were analyzed using the Odyssey Application Software to obtain the integrated fluorescence intensities.

Caspase-3/7 activity

HUVECs were plated in 96-well cell culture dishes. When cells reached 80% confluence, they were treated as described above. Then, Caspase-Glo® 3/7 reagent was added to the plates and incubated for 30 min at room temperature following the manufacturer's protocols. The absorbance was measured immediately at 520 nm using an FLx800™ Multi-Detection Microplate Reader (Bio-Tek).

Lactate dehydrogenase (LDH) assay

After treatment, cell culture medium was collected and centrifuged at 400 × *g* for 10 min. Then, the suspension was transferred to a new 96-well plate for LDH assay following the manufacturer's protocols. The absorbance of the reaction mixture was measured at 340 nm using an FLx800™ Multi-Detection Microplate Reader (Bio-Tek).

Transmission electron microscopy

HUVECs were seeded into 100-mm culture dishes. When the cells reached 80% confluence, they were treated with DMSO or 20 μM curcumin analog A2 for 6 h. Then, the cells were fixed, dehydrated, embedded, sectioned, and stained according to previously reported methods [19]. Ultrathin sections of these samples were observed under a JEM-1230 transmission electron microscope (JEOL Co., Ltd., Japan).

Immunofluorescence staining

After treatment, cells were fixed in 4% paraformaldehyde for 15 min at 4 °C and blocked in 5% BSA for 30 min. Then, the cells were incubated with anti-LC3B (1:500) primary antibody overnight at 4 °C and subsequently incubated with the appropriate secondary antibody. Nuclei were stained with DAPI for 15 min. Fluorescence images were captured using a confocal laser-scanning microscope (Olympus FLUOVIEW FV3000). Different fields of view (>5 regions) were analyzed on the confocal laser-scanning microscope for each labeling condition, and representative results are shown.

Quantitative real-time PCR (qRT-PCR)

qRT-PCR was carried out as previously reported [20]. The specific primers are listed below: GAPDH-F, 5′-AATGACCCCTTCATTGAC-3'; GAPDH-R, 5′-TCCACGACGTACTCAGCGC-3′; SQSTM1-F, 5′-TACGACT TGTGTAGCGTCTGC-3′; and SQSTM1-R, 5′-GTGTCCGTGTTTCACCT TCC-3′.

Autophagy flux assay

Autophagy flux was detected using the Premo™ Autophagy Tandem Sensor RFP-GFP-LC3B Kit according to the manufacturer's instructions. Briefly, HUVECs were plated in 6-well culture dishes. When the cells reached 60% confluence, they were incubated with 12 μL BacMam Reagents containing RFP-GFP-LC3B for 16 h. Then, the cells were treated as described above. Fluorescence images were captured using a fluorescence microscope (Leica, Wetzlar, Hessen, Germany). Autophagosomes (green) and autophagolysosomes (red) were quantified using ImageJ.

Measurement of reactive oxygen species (ROS) levels

HUVECs were plated in 100-mm culture dishes. When the cells reached 80% confluence, they were treated as described above. To determine intracellular ROS levels, we used DCFH-DA probes. To measure mitochondrial ROS production, we used the fluorogenic dye MitoSOX® Red. After treatment, the cells were incubated with 10 μM DCFH-DA or 5 μM MitoSOX® Red for 20 min and collected for flow cytometry (BD FACSCalibur).

Mitochondrial membrane potential (MMP) measurement

MMP was measured using the mitochondrial probe JC-1. JC-1 aggregates together to form polymers emitting red fluorescence signals in hyperpolarized mitochondria. If the mitochondrial

membrane is depolarized, JC-1 exists as monomers emitting green fluorescence signals. After treatment, HUVECs were incubated with 4 μg/mL JC-1 for 15 min and photographed under a fluorescence microscope (Leica, Wetzlar, Hessen, Germany) or analyzed using flow cytometry (BD FACSCalibur).

Statistical analysis

All experiments were performed in duplicate and repeated at least three times. The results were expressed as the means ± standard error of the mean (SEM). Differences between groups were analyzed by one-way variance (ANOVA), and the means of two groups were compared using Student's *t*-test with SPSS (version 17.0). Differences at $P < 0.05$ were considered statistically significant.

RESULTS

Curcumin analog A2 exhibits potent antiangiogenic activity in vitro, ex vivo, and in vivo

As the migration of VECs is an essential step for new blood vessel formation, we screened a series of monocarbonyl analogs of curcumin for their antiangiogenic activity in vitro using cell monolayer wound healing assays. Among the analogs examined, curcumin analog A2 (Fig. 1) at concentrations of 20 or 40 μmol/L completely inhibited VEC migration (Fig. 2a). Therefore, curcumin analog A2 was selected as a hit compound for further study.

The formation and merging of tubes by VECs is another crucial step in the process of angiogenesis, which is required for the formation of a complex network of vessels and capillaries [21]. We used the Matrigel tube formation assay, an ideal in vitro model

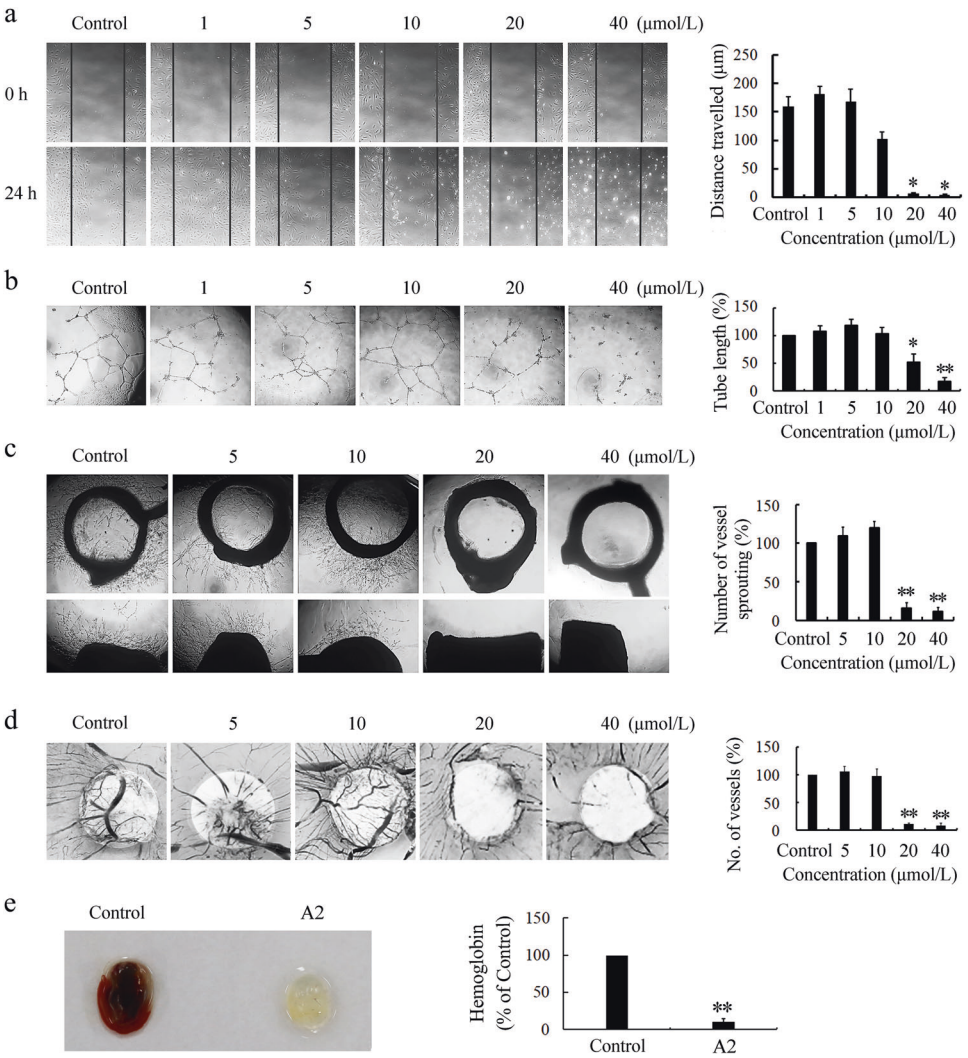

Fig. 2 Curcumin analog A2 inhibits angiogenesis in vitro, ex vivo, and in vivo. **a** The effect of curcumin analog A2 on the migration of human umbilical vein endothelial cells (HUVECs) was determined using wound healing assay. These photos were taken under a phase-contrast microscope (×40). Top photos were taken immediately after scraping. Bottom photos were taken at 24 h after scraping. Histogram shows the cell migration distance data. ($n = 3$; $^{*}P < 0.05$ vs. Control). **b** The effect of curcumin analog A2 on the tube formation of HUVECs was detected by plating cells on Matrigel. These photos were taken at 24 h after treatment under a phase-contrast microscope (×40). Histogram shows the relative total length of tubes. ($n = 3$; $^{*}P < 0.05$; $^{**}P < 0.01$ vs. Control). **c** The effect of curcumin analog A2 on the vessel sprouting was measured using rat aortic rings assay. These photos were taken at day 7 after treatment under a phase-contrast microscope (×40). Top photos show the aortic rings placed horizontally in Matrigel. Bottom photos show the aortic rings placed vertically in Matrigel. Histogram shows the relative total number of vessels sprouting. ($n = 3$; $^{**}P < 0.01$ vs. Control). **d** The effect of curcumin analog A2 on the new blood vessels formation was detected using chicken CAM assay. These photos were taken using a Canon EOS 550D Digital SLR camera. Histogram shows the relative number of new blood vessels on the filter paper disks. ($n = 3$; $^{**}P < 0.01$ vs. Control). **e** The effect of curcumin analog A2 on the neovascularization was detected using Matrigel plug assay. On day 14, Matrigel plugs were harvested and photographed using a Canon EOS 550D Digital SLR camera. Histogram shows the relative hemoglobin contents in the Matrigel plugs. ($n = 3$; $^{**}P < 0.01$ vs. Control)

system to study the formation of vascular loops to detect whether curcumin analog A2 affects VEC tube formation. The results showed that curcumin analog A2 at concentrations equal to or above 20 μM dramatically reduced the number of branch points of tubules and total tube length (Fig. 2b).

The effect of curcumin analog A2 on tube formation cannot be directly translated into its in vivo antiangiogenic activity; thus, we further explored the effects of curcumin analog A2 on angiogenesis using ex vivo and in vivo models. First, we found that compared with the control, curcumin analog A2 at concentrations equal to or above 20 μM markedly suppressed neovessel sprouting at the cut edge of rat aortic rings (Fig. 2c). Second, we found using chick CAM assays that the formation of new blood vessels was significantly blocked by curcumin analog A2 (20 or 40 μM), which even induced a vascular zone in the developing embryos (Fig. 2d). Third, 20 μM curcumin analog A2 almost completely inhibited vascularity in the Matrigel plugs (Fig. 2e), confirming its potent antiangiogenic efficacy in vivo.

Curcumin analog A2 induces death in HUVECs

Considering that VEC survival is critical for angiogenesis, we next investigated whether curcumin analog A2-induced cell death in HUVECs. Using a phase-contrast microscope, we observed that compared with the control, curcumin analog A2 at concentrations >10 μM gradually increased the number of shrinking cells and cells detaching from culture dishes (Supplementary Fig. 1). Notably, extensive cytoplasmic vacuolization was the earliest morphological change in response to curcumin analog A2 treatment in HUVECs (Supplementary Fig. 1). Next, the number of HUVECs exposed to various concentrations of curcumin analog A2 was monitored using real-time cell analysis (RTCA). The results showed that curcumin analog A2 reduced the number of HUVECs in a dose-dependent manner (Fig. 3a). Similar results were obtained using MTT assays (Fig. 3b). To further corroborate the cytotoxic effect of curcumin analog A2 on HUVECs, we performed an annexin V/propidium iodide (PI) double-staining assay using flow cytometric analysis. Curcumin analog A2 increased the

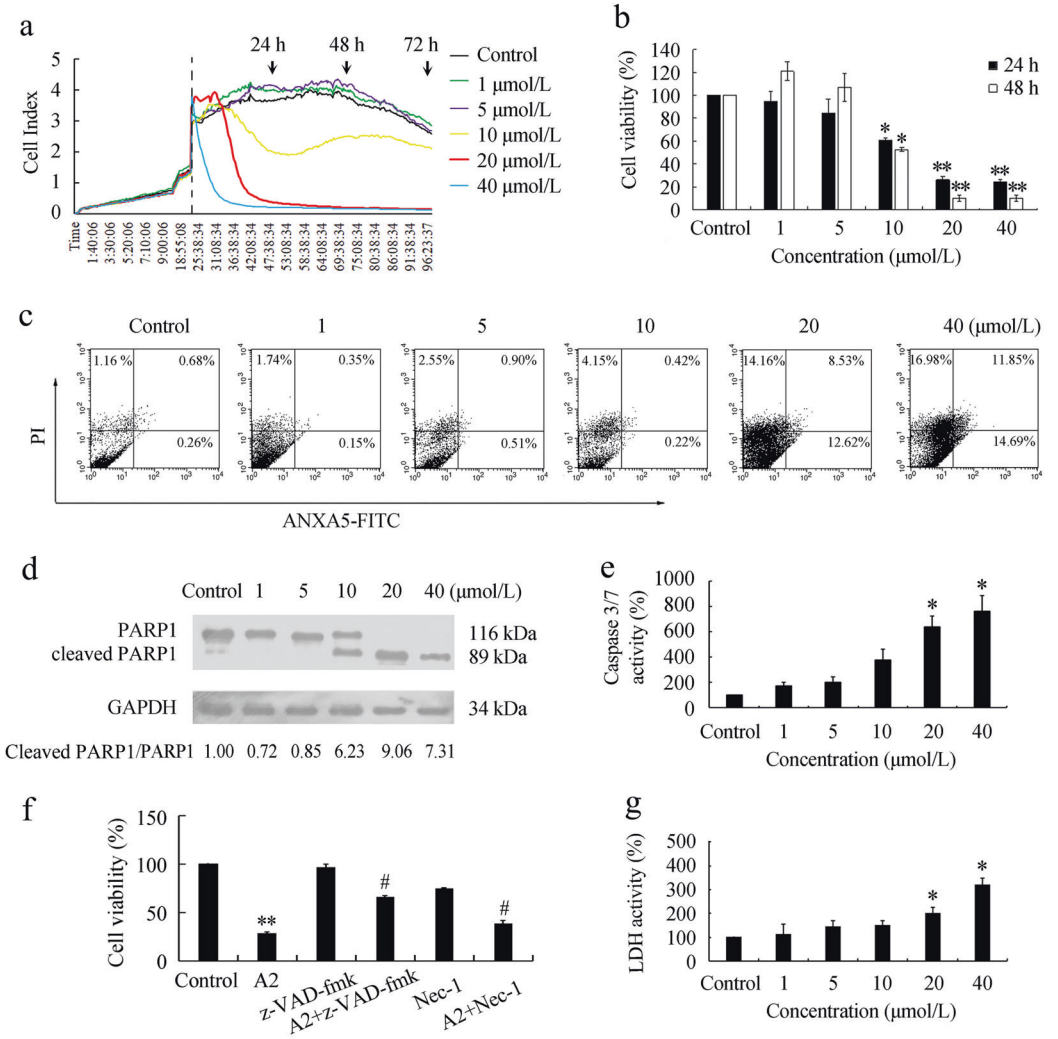

Fig. 3 Curcumin analog A2 induces cell death in human umbilical vein endothelial cells (HUVECs). **a** Cell viability was monitored over 96 h in real-time using an xCELLigence RTCA S16 System. Cell-sensor impedance is displayed as the cell index. The vertical dotted line indicates dimethyl sulfoxide (DMSO) or curcumin analog A2 addition time points. **b** Cell viability was detected using MTT assay. HUVECs were treated with DMSO or curcumin analog A2 for 24 or 48 h, respectively. ($n = 3$; $^{*}P < 0.05$; $^{**}P < 0.01$ vs. Control). **c** Flow cytometric analysis of ANXA5-FITC/PI staining in HUVECs treated with DMSO or curcumin analog A2 for 24 h. **d** Western blot analysis of the cleavage of PARP1 in HUVECs treated with curcumin analog A2 for 24 h. **e** Histogram shows the relative activities of caspase-3/7 in HUVECs treated with DMSO or curcumin analog A2 for 24 h. ($n = 3$; $^{*}P < 0.05$ vs. Control). **f** Cell viability was detected using MTT assay. HUVECs were preincubated with z-VAD-fmk (20 μM) or necrostatin-1 (Nec-1; 100 μM) for 1 h, then they were treated with DMSO or curcumin analog A2 (20 μM) for 24 h. ($n = 3$; $^{**}P < 0.01$ vs. Control; $^{\#}P < 0.05$ vs. A2). **g** Bar graph shows the relative lactate dehydrogenase (LDH) activity in HUVECs treated with DMSO or curcumin analog A2 for 24 h. ($n = 3$; $^{*}P < 0.05$ vs. Control)

proportion of PI-positive or annexin V-positive cells (Fig. 3c) in a dose-dependent manner, confirming that it could induce cell death in HUVECs.

Next, we investigated whether curcumin analog A2-induced apoptosis in HUVECs. We found that curcumin analog A2 at concentrations equal to or above 20 μM obviously induced PARP1 cleavage (Fig. 3d), which is a central event in the execution of the apoptotic program. In addition, caspase-3/7 activities in curcumin analog A2 (10 or 20 μM)-treated cells were higher than those in untreated cells (Fig. 3e). Curcumin analog A2 (20 μM)-induced high death rates in HUVECs could be partially reversed by pretreatment with z-VAD-FMK, indicating that curcumin analog A2 not only induced apoptosis but also nonapoptotic endothelial cell death. Pretreatment with necrostatin-1, an inhibitor of RIP1 kinase, also partially reversed curcumin analog A2 (20 μM)-induced cell death in HUVECs (Fig. 3f). In addition, curcumin analog A2 increased PI uptake (Fig. 3c) and LDH release (Fig. 3g) in HUVECs. These data suggested that curcumin analog A2 induced both necroptosis and apoptosis.

Curcumin analog A2 enhances autophagic activity in HUVECs

To understand the nature of the vesicles observed in curcumin analog A2-treated cells, we first stained HUVECs with AO. A higher number of red fluorescent dots, which represent acidic compartments, were observed in the cytoplasm of curcumin analog A2-treated cells than in the cytoplasm of control cells (Supplementary Fig. 2). The increase in acidic compartments prompted us to address the possibility that curcumin analog A2 might affect the process of autophagy in HUVECs. MAP1LC3B/LC3B is a classic marker used to monitor autophagic activity. When autophagy occurs, LC3B undergoes a molecular conversion from cytoplasmic LC3B-I into its lipidated counterpart LC3B-II, which is recruited to phagophores and remains tightly bound to the inner membrane of the autophagosome until it is degraded in the autolysosome [22]. We detected the distribution of LC3B using immunostaining assays. Treatment of HUVECs with curcumin analog A2 for 6 h increased the number of LC3B-positive puncta in a dose-dependent manner (Fig. 4a). For further evidence of curcumin analog A2-regulated autophagy, we carried out ultrastructural investigation to visualize autophagic vacuoles. Double-membrane autophagosomes could be observed in curcumin analog A2-treated HUVECs (Fig. 4b). Moreover, autophagy can be monitored by the detection of LC3B processing and LC3B-II accumulation. We found that the treatment of HUVECs with curcumin analog A2 increased the level of LC3B-II in dose- and time-dependent manners (Fig. 4c).

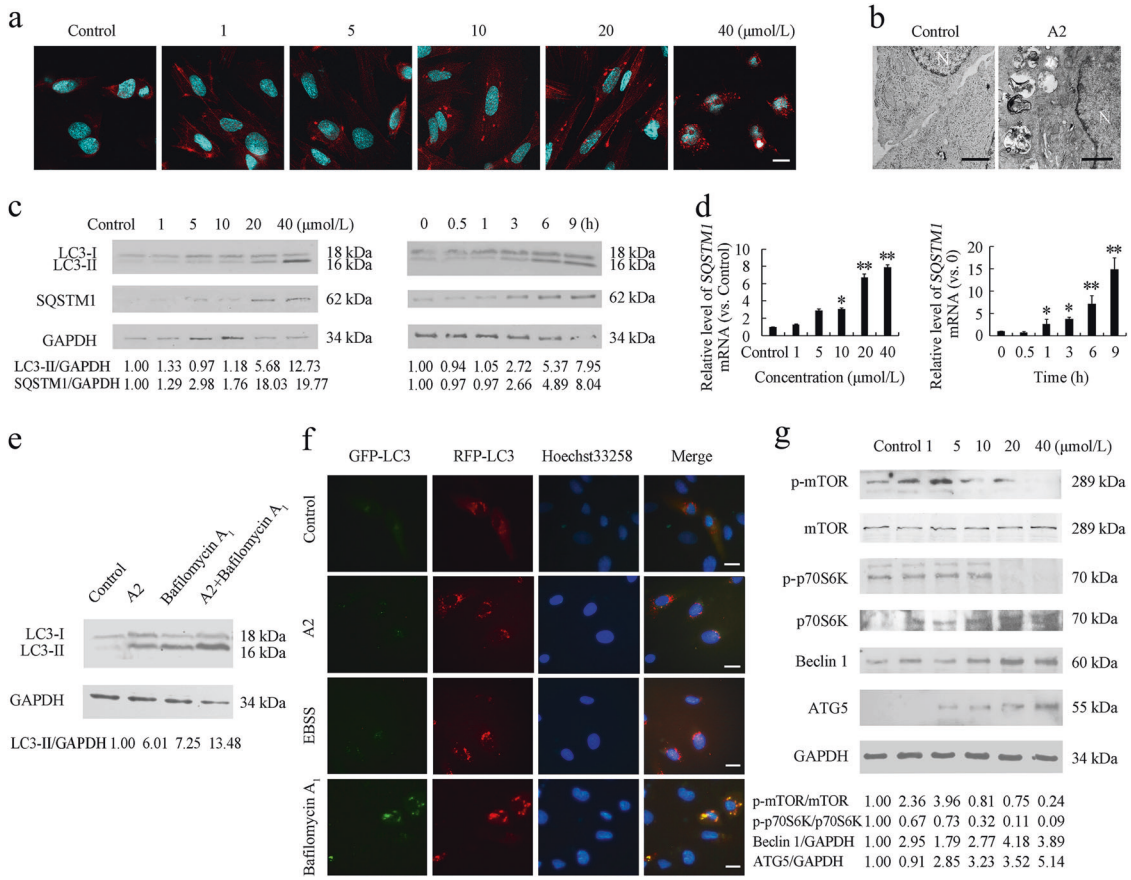

Fig. 4 Curcumin analog A2 induces autophagy in human umbilical vein endothelial cells (HUVECs). **a** Fluorescence photographs of endogenous LC3B puncta in HUVECs treated with curcumin analog A2 for 6 h. Nuclei were stained with DAPI. Scale bar: 10 μm. **b** Transmission electron microscopy images of HUVECs treated with dimethyl sulfoxide (DMSO) or curcumin analog A2 for 6 h. Scale bar: 500 nm. **c** Western blot analysis of LC3B-II and SQSTM1 levels in HUVECs treated with DMSO or curcumin analog A2 for 6 h, or in the cells treated with curcumin analog A2 (20 μM) for 0–9 h. **d** Quantitative real-time PCR (qRT-PCR) analysis of SQSTM1 mRNA level in HUVECs treated with DMSO or curcumin analog A2 for 6 h, or in the cells treated with curcumin analog A2 (20 μM) for 0–9 h. ($n = 3$; *$P < 0.05$; **$P < 0.01$ vs. Control). **e** Western blot analysis of LC3-II levels in HUVECs treated with DMSO or curcumin analog A2 (20 μM) in the absence or presence of bafilomycin A_1 (100 nM) for 6 h. **f** Fluorescence photographs of HUVECs transfected with RFP-GFP-LC3B plasmid. Cells were treated with DMSO or curcumin analog A2 (20 μM) in complete medium or EBSS for 6 h. Bafilomycin A1 (100 nM)-treated cells were used as positive controls. Nuclei were stained with Hoechst 33258. Scale bar: 10 μm. **g** Western blot analysis of p-mTOR, p-P70S6K, Beclin1 and ATG5 levels in HUVECs treated with DMSO or curcumin analog A2 for 6 h

The increase in the number of autophagosomes and level of LC3B-II can be due to an increased autophagic activity or impairment of autophagosome degradation. To uncover the real effect of curcumin analog A2 on autophagy, we next evaluated autophagy flux. SQSTM1 (sequestosome 1) is recruited to autophagosomes and constitutively degraded during autophagy. Increased protein levels of SQSTM1 commonly reflect an impairment of autophagosome degradation. Western blot analysis showed that the protein level of SQSTM1 was elevated in curcumin analog A2-treated HUVECs (Fig. 4c). However, curcumin analog A2 also significantly increased SQSTM1 mRNA levels (Fig. 4d). Thus, it was difficult to distinguish whether the increase in SQSTM1 protein levels was due to the impairment of autophagy flux or the inhibitory effects of curcumin analog A2 on SQSTM1 expression.

If curcumin analog A2 induces autophagy, late-stage autophagy inhibitors, such as bafilomycin A1, are expected to further increase the level LC3B-II. HUVECs treated with curcumin analog A2 and bafilomycin A_1 had higher levels of LC3B-II than cells treated with curcumin analog A2 or bafilomycin A_1 alone (Fig. 4e), suggesting that curcumin analog A2 acts by inducing autophagosome formation rather than by blocking autophagy flux. Autophagy flux was further detected using RFP-GFP-LC3B plasmids. GFP (green fluorescent protein) but not RFP (red fluorescent protein) loses its fluorescence in acidic lysosomes. Thus, autophagosomes are labeled as yellow puncta (the overlay of green and red fluorescence), while autolysosomes are only labeled as red puncta. The increase in both yellow and red puncta indicates enhanced autophagic activity. We observed many yellow puncta but very few red puncta in bafilomycin A1-treated cells, indicating an inefficient degradation of autophagosomes. In contrast, 20 μM curcumin analog A2 increased the number of both yellow and red puncta in HUVECs, which was similar to the effects of incubation with EBSS (Fig. 4f and Supplementary Fig. 3). Moreover, we investigated whether curcumin analog A2 influences the levels of key regulators of autophagy induction, such as p-mTOR, p-P70S6K, Beclin1 and ATG5. As shown in Fig. 4g, the levels of p-mTOR and p-P70S6K were decreased, while the levels of Beclin1 and ATG5 were increased in curcumin analog A2-treated HUVECs. These results collectively demonstrated that curcumin analog A2-induced autophagy in HUVECs.

Curcumin analog A2-induced autophagy does not affect its cytotoxicity toward HUVECs

To evaluate whether curcumin analog A2-induced autophagy is a protective response or an essential process, leading to cell death, we used the autophagy inhibitor wortmannin or specific siRNAs against ATG5 to block curcumin analog A2-induced autophagy (Supplementary Fig. 4). Data from real-time cell analysis showed that there was no obvious difference in cell number between curcumin analog A2-treated normal cells and wortmannin-treated or ATG5 siRNA-transfected cells (Fig. 5a, b). Similarly, suppression of autophagy by wortmannin or transfection with ATG5 siRNAs neither reduced nor aggravated curcumin analog A2-induced cell death (Fig. 5c, d).

We further detected whether the suppression of autophagy affected curcumin analog A2-induced apoptosis and necroptosis in HUVECs. The data showed that blockade of autophagy by wortmannin or transfection with ATG5 siRNAs did not affect either the cleavage of PARP1 or LDH release (Fig. 5e, f). Collectively, these data suggested that curcumin analog A2-induced autophagy did not influence its cytotoxic effects toward HUVECs.

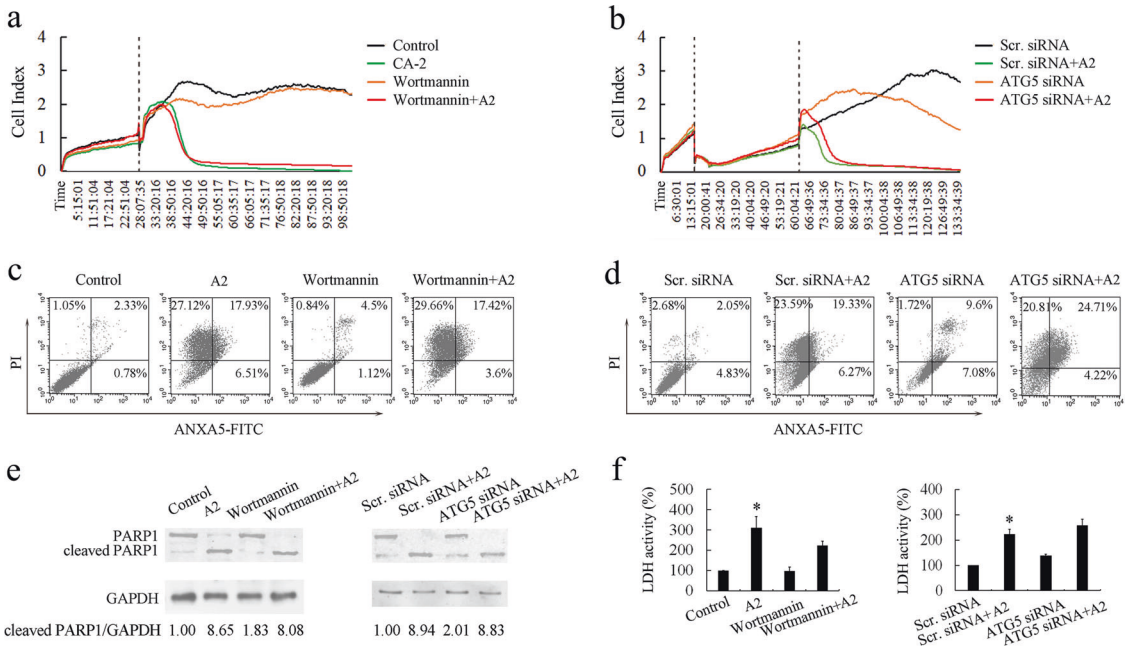

Fig. 5 Curcumin analog A2-induced human umbilical vein endothelial cell (HUVEC) death is neither accelerated nor delayed by autophagy inhibition. **a** Cell viability was monitored over 96 h in real-time using an xCELLigence RTCA S16 System. Cell-sensor impedance is displayed as the cell index. The vertical dotted line indicates dimethyl sulfoxide (DMSO), curcumin analog A2 (20 μM) or wortmannin (2 μM) addition time points. **b** Cell viability was monitored over 133 h in real-time using an xCELLigence RTCA S16 System. Cell-sensor impedance is displayed as the cell index. The first vertical dotted line indicates small-interfering RNAs (siRNAs) transfection time points, the second vertical dotted line indicates DMSO or curcumin analog A2 (20 μM) addition time points. **c** Flow cytometric analysis of ANXA5-FITC/PI staining in HUVECs treated with DMSO or curcumin analog A2 (20 μM) in the presence or absence of wortmannin (2 μM) for 24 h. **d** Flow cytometric analysis of ANXA5-FITC/PI staining in scrambled siRNA or ATG5 siRNA-transfected HUVECs treated with DMSO or curcumin analog A2 (20 μM) for 24 h. **e** Western blot analysis of the cleavage of PARP1 in HUVECs treated as indicated for 24 h. **f** Bar graph shows the relative lactate dehydrogenase (LDH) activity in HUVECs treated as indicated for 24 h. ($n = 3$; $^*P < 0.05$ vs. Control)

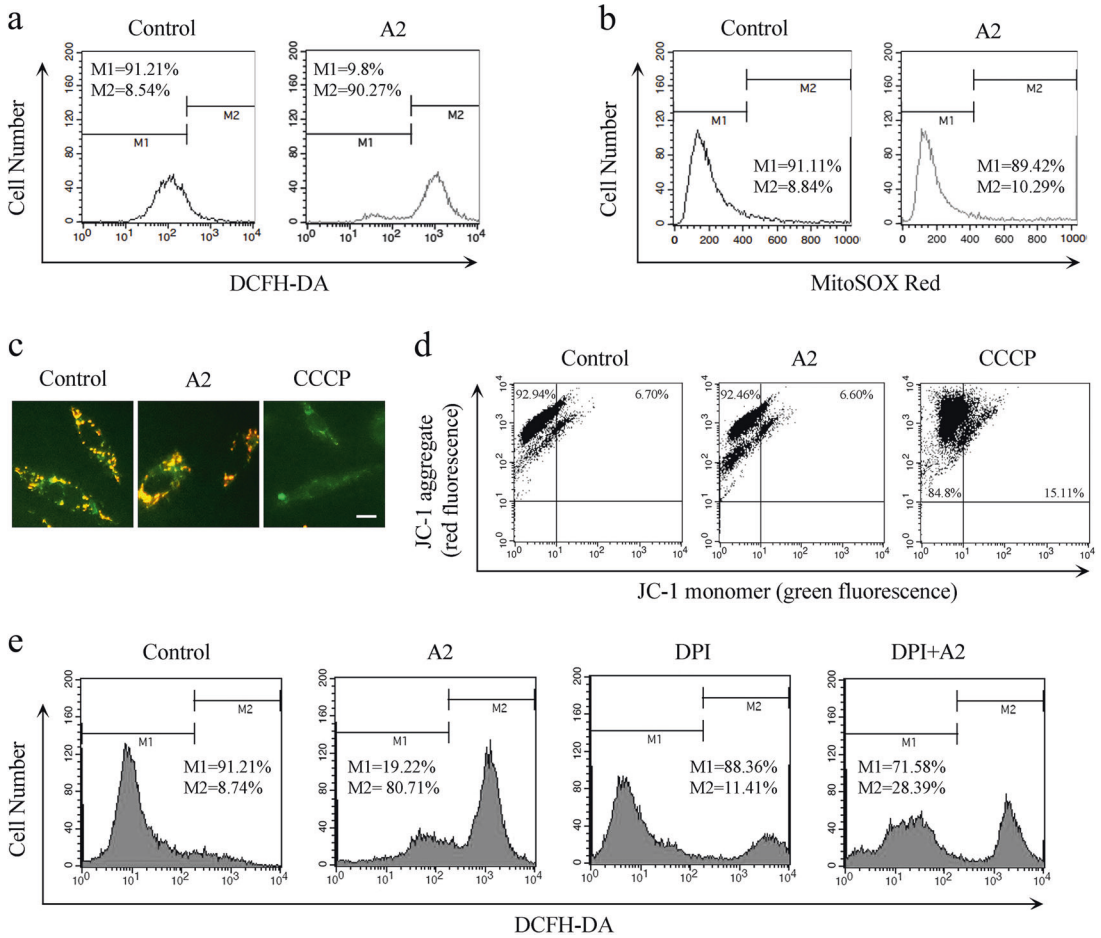

Fig. 6 Curcumin analog A2 increased the level of NADH/NADPH oxidase-derived reactive oxygen species (ROS). **a** Flow cytometric analysis of the intracellular ROS levels. Human umbilical vein endothelial cells (HUVECs) were treated with dimethyl sulfoxide (DMSO) or curcumin analog A2 (20 μM) for 3 h, then the cells were loaded with 10 μM DCFH-DA for 20 min. **b** Flow cytometric analysis of the mitochondrial ROS levels. HUVECs were treated with DMSO or curcumin analog A2 (20 μM) for 3 h, then the cells were loaded with 5 μM MitoSOX® Red for 20 min. **c** Fluorescence photographs of JC-1 staining in HUVECs treated with DMSO or curcumin analog A2 (20 μM) for 6 h. CCCP-treated cells were used as positive controls. Scale bar: 10 μm. **d** Flow cytometric analysis of JC-1 staining in HUVECs treated with DMSO or curcumin analog A2 (20 μM) for 6 h. CCCP-treated cells were used as positive controls. **e** Flow cytometric analysis of the intracellular ROS levels. HUVECs were treated with DMSO or curcumin analog A2 (20 μM) in the presence or absence of DPI for 3 h, then the cells were loaded with 10 μM DCFH-DA for 20 min

ROS are directly involved in curcumin analog A2-induced cell death and autophagy in HUVECs

ROS play important roles in intracellular signal transduction and homeostasis. However, excessive ROS production is toxic, which causes damage to main cellular components and subsequent cell death [23]. To detect whether curcumin analog A2-induced cytotoxicity is associated with changes in the intracellular redox environment, we first examined the levels of intracellular ROS. Data from flow cytometry using the DCFH-DA probe showed that curcumin analog A2 markedly elevated ROS levels (Fig. 6a). Mitochondria and NADH/NADPH oxidase are the two major sources of ROS production. We found that curcumin analog A2 did not influence the level of mitochondrial ROS or MMP (Fig. 6b–d), excluding the possibility that curcumin analog A2 increases ROS levels in HUVECs via the mitochondria. Then, we preincubated the cells with DPI, a specific inhibitor of NADH/NADPH oxidase. We found that DPI markedly inhibited ROS production in curcumin analog A2-treated HUVECs (Fig. 6e). These data suggested that curcumin analog A2-induced ROS are derived, at least partially, from NADH/NADPH oxidase and not the mitochondria.

Next, we investigated whether curcumin analog A2-induced ROS are involved in its cytotoxicity. MTT assay results revealed that the removal of ROS by NAC markedly reversed the curcumin analog A2-induced reduction in HUVEC viability (Fig. 7a). Pretreatment with NAC effectively reduced PARP1 cleavage and LDH release in curcumin analog A2-treated HUVECs, indicating that ROS are required for curcumin analog A2-induced apoptosis and necroptosis (Fig. 7b, c). These results were further supported by annexin V-PI double-staining assays using flow cytometric analysis (Fig. 7d).

Moreover, we detected whether ROS are associated with curcumin analog A2-induced autophagy. Western blot analysis showed that scavenging ROS with NAC abolished curcumin analog A2-induced increase in the levels of LC3B-II (Fig. 7e). NAC also suppressed the mRNA level of LC3B in curcumin analog A2-treated HUVECs (Supplementary Fig. 5). It was, therefore, unclear whether the reduction in LC3B-II protein levels was due to the antagonistic effect of removing ROS on curcumin analog A2-induced autophagy or the inhibitory effect of NAC on LC3B-II levels through a posttranslational mechanism. To solve this problem, HUVECs were transfected with exogenous RFP-GFP-LC3B reporters. We found that NAC treatment effectively suppressed the number of both red and yellow puncta in curcumin analog A2-treated HUVECs (Fig. 7f and Supplementary Fig. 6), indicating that ROS generation was required for curcumin analog A2-induced autophagy.

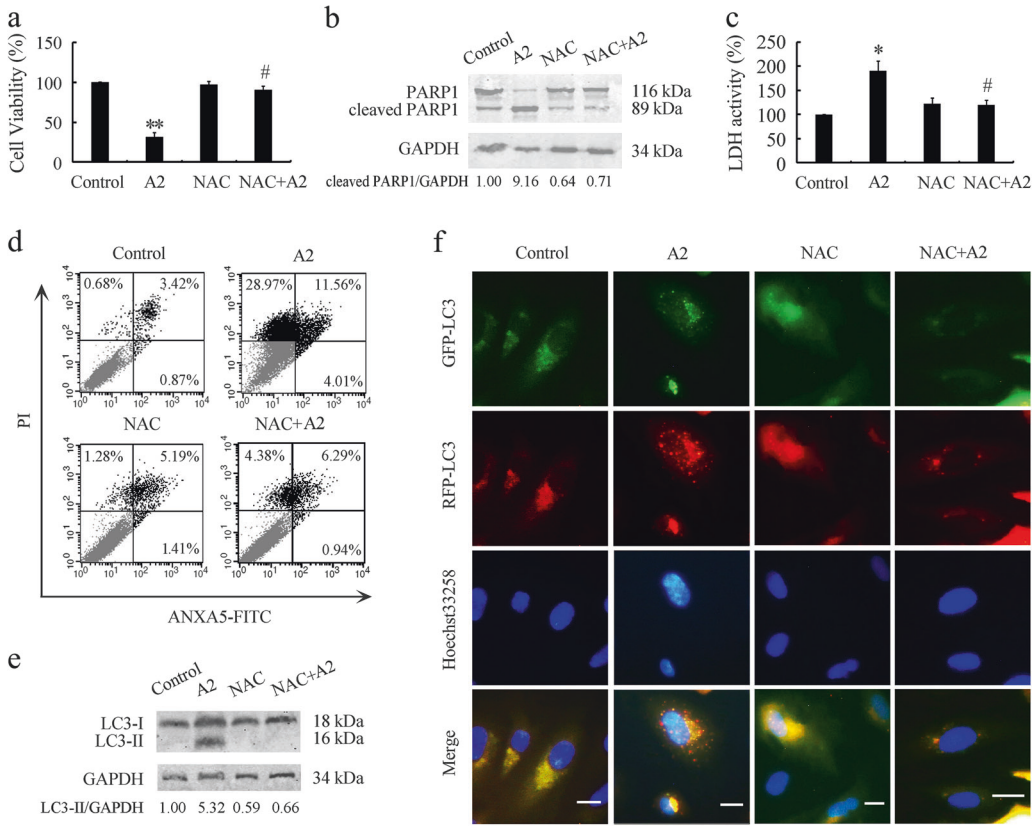

Fig. 7 Scavenging reactive oxygen species (ROS) reverses curcumin analog A2-induced cell death and autophagy in human umbilical vein endothelial cells (HUVECs). HUVECs were preincubated with NAC (10 mM) for 1 h, then they were treated with dimethyl sulfoxide (DMSO) or curcumin analog A2 (20 μM) for 24 h. **a** Cell viability was detected using MTT assay. ($n = 3$; $^{**}P < 0.01$ vs. Control; $^{\#}P < 0.05$ vs. A2). **b** Western blot analysis of the cleavage of PARP1. **c** Bar graph shows the relative lactate dehydrogenase (LDH) activity. ($n = 3$; $^{*}P < 0.05$ vs. Control; $^{\#}P < 0.05$ vs. A2). **d** Flow cytometric analysis of ANXA5-FITC/PI staining. **e** Western blot analysis of LC3B-II levels. **f** Fluorescence photographs of HUVECs transfected with RFP-GFP-LC3B plasmid. Scale bar: 10 μm

Scavenging ROS reverses the antiangiogenic activity of curcumin analog A2 in vitro, ex vivo, and in vivo

Additional experiments were performed to investigate the role of ROS in the antiangiogenic activity of curcumin analog A2. We found that scavenging ROS with NAC completely reversed the inhibitory effect of curcumin analog A2 (20 μM) on the migration and tube formation of HUVECs (Fig. 8a, b), suggesting that ROS are essential for the antiangiogenic activity of curcumin analog A2 in vitro. Furthermore, quantification of three independent rat aortic ring assays revealed that the inhibitory effects of curcumin analog A2 (20 μM) on angiogenesis were efficiently suppressed by NAC treatment (Fig. 8c). Similar results were obtained using chicken CAM assays (Fig. 8d). These data collectively suggested that curcumin analog A2 inhibited angiogenesis through a ROS-mediated mechanism.

DISCUSSION

Cancer cell survival, seeding, or metastatic outgrowth all require neoangiogenesis to deliver oxygen, nutrients, and growth factors. Deregulation of vessel growth is a main driving force in the progression of cancer [24]. Many critical steps are involved in the process of angiogenesis and capillary network formation, including endothelial cell survival, proliferation, migration, organization, and remodeling into capillary-like structures [25]. Thus, endothelial cells play a crucial role in the progression of cancer by controlling angiogenesis. In the current study, after screening, we found that monocarbonyl curcumin analog A2 at concentrations equal to or above 20 μM significantly inhibited endothelial cell migration and tube formation in vitro, inhibited neovessel sprouting at the cut edge of rat aortic rings ex vivo, and strongly blocked newly formed microvessels in CAMs and Matrigel plugs in vivo. These results collectively demonstrated that curcumin analog A2 is a potent antiangiogenic compound. The antiangiogenic mechanism is illustrated in Fig. 9.

Induction of endothelial cell apoptosis is believed to be one of the core mechanisms of antiangiogenic therapies [26, 27]. As expected, curcumin analog A2-induced HUVEC apoptosis as evidenced by the increase in PARP1 cleavage, caspase-3/7 activities and inhibitory effect of Z-VAD-FMK, a pancaspase inhibitor. However, the cell death induced by curcumin analog A2 was not completely reversed by Z-VAD-FMK pretreatment, suggesting that curcumin analog A2 induced both nonapoptotic cell death and apoptosis in HUVECs. Additionally, 20 μM curcumin analog A2-induced PI uptake and LDH release, indicating the rupture of the cell membrane. Treatment of HUVECs with Nec-1, a specific necroptosis inhibitor, attenuated the cytotoxic effect of curcumin analog A2. These data collectively suggested that curcumin analog A2 induced both apoptosis and necroptosis in HUVECs.

Curcumin analog A2 was found to induce cytoplasmic vacuolation, which was identified by acidic compartments exhibiting strong AO staining, before ultimate cell death. Furthermore, we found that curcumin analog A2 increased the number of autophagosomes and the level of LC3B-II, suggesting that curcumin analog A2 likely triggered autophagy in HUVECs. In the presence of the late-stage autophagy inhibitor bafilomycin A_1, curcumin analog A2 further increased LC3B-II levels, indicating

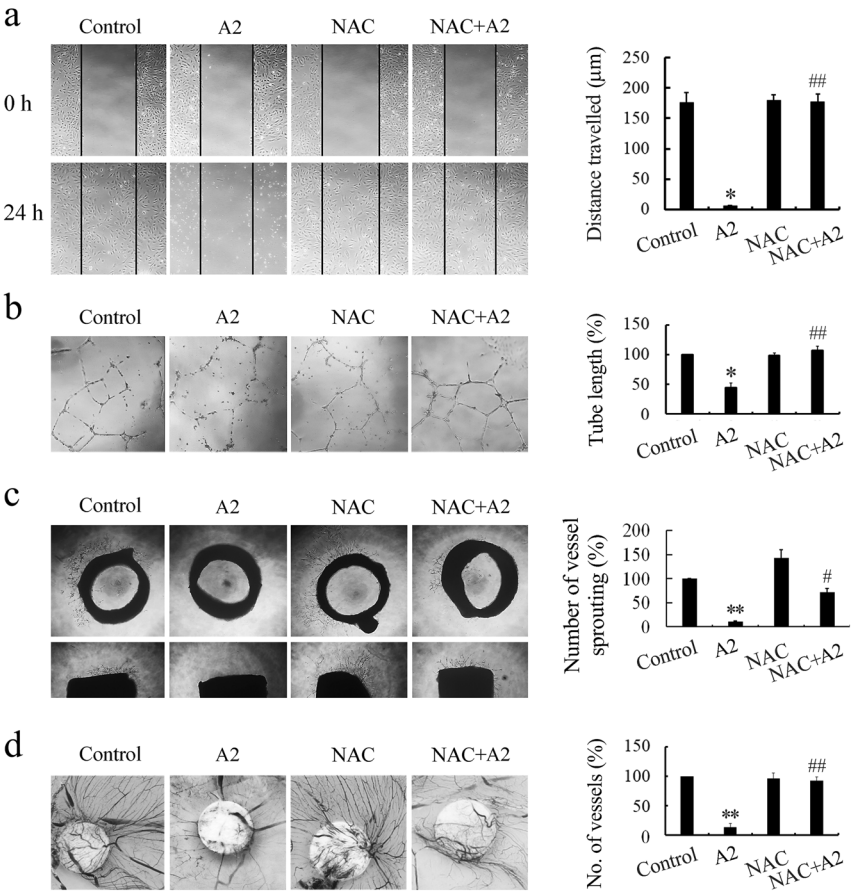

Fig. 8 Scavenging reactive oxygen species (ROS) reverses the antiangiogenic effects of curcumin analog A2 in vitro, ex vivo, and in vivo. **a** Wound healing assay was used to assess the migration of human umbilical vein endothelial cells (HUVECs) treated with dimethyl sulfoxide (DMSO) or curcumin analog A2 (20 μM) in the presence or absence of NAC (10 mM). These photos were taken under a phase-contrast microscope (×40). Top photos were taken immediately after scraping. Bottom photos were taken at 24 h after scraping. Histogram shows the cell migration distance data. ($n = 3$; $^{*}P < 0.05$ vs. Control; $^{\#\#}P < 0.01$ vs. A2). **b** HUVECs were plated on Matrigel, then the cells were treated with DMSO or curcumin analog A2 (20 μM) in the presence or absence of NAC (10 mM) for 24 h. These photos were taken at 24 h after treatment under a phase-contrast microscope (×40). Histogram shows the relative total length of tubes. ($n = 3$; $^{*}P < 0.05$ vs. Control; $^{\#\#}P < 0.01$ vs. A2). **c** Rat aortic rings were incubated with DMSO or curcumin analog A2 (20 μM) in the presence or absence of NAC (10 mM). These photos were taken at day 7 after treatment under a phase-contrast microscope (×40). Top photos show the aortic rings placed horizontally in Matrigel. Bottom photos show the aortic rings placed vertically in Matrigel. Histogram shows the relative total number of vessels sprouting. ($n = 3$; $^{**}P < 0.01$ vs. Control; $^{\#}P < 0.05$ vs. A2). **d** New blood vessels formation was detected using chicken CAM assay. Sterilized filter paper disks saturated with DMSO or curcumin analog A2 (20 μM) in the presence or absence of NAC (10 mM) were placed on the CAMs. After incubation for 2 days, the CAMs were removed for further analysis. These photos were taken using a Canon EOS 550D Digital SLR camera. Histogram shows the relative number of new blood vessels on the filter paper disks. ($n = 3$; $^{**}P < 0.01$ vs. Control; $^{\#\#}P < 0.01$ vs. A2)

that curcumin analog A2 enhanced autophagic activity rather than block autophagosome degradation. This notion was further confirmed by transfection of HUVECs with RFP-GFP-LC3B plasmids, which phenocopied the results obtained with EBSS incubation. Western blot analysis showed that curcumin analog A2 increased the levels of Beclin1 and ATG5 and attenuated the phosphorylation of mTOR and its downstream target P70S6K. It is plausible that these autophagy-related proteins might be involved in curcumin analog A2-induced autophagy. However, further studies are needed to verify this hypothesis.

Autophagy proceeds at a basal level under physiological conditions in vascular endothelial cells to maintain cellular homeostasis [28]. Recent studies have shown that autophagic responses can be triggered in vascular endothelial cells by a variety of antiangiogenic agents [28]. Although some antiangiogenic agents have been demonstrated to induce autophagic cell death in vascular endothelial cells, it is suggested that in most situations, induction of autophagy exerts cytoprotective effects on vascular endothelial cells, and this acts as an important cellular mechanism of drug resistance [28–30]. For instance, the antiangiogenic agent sulforaphane (SUL) induces both autophagy and apoptosis in HUVECs. Inhibition of autophagy potentiates the proapoptotic effect of SUL [31]. Similarly, autophagy triggered by the antiangiogenic agent BA145 can weaken its cytotoxicity toward HUVECs and subsequently contribute to the acquired resistance to this compound [29]. We are reporting for the first time that curcumin analog A2-induced autophagy in HUVECs is neither a prerequisite for toxicity, leading to cell death nor a protective response for combating the toxicity due to curcumin analog A2. These data clearly suggest that although the combination of antiangiogenic agents with autophagy inhibitors constitutes an effective therapeutic approach against cancer, it is not suitable in all cases.

Oxidative stress resulting from the overproduction of ROS might serve as one of the common inducers of endothelial cell death in tumors [32]. One possible explanation is that vascular endothelial cells in the tumor microenvironment generally exhibit elevated ROS levels caused by metabolic abnormalities. Thus, tumor vessel

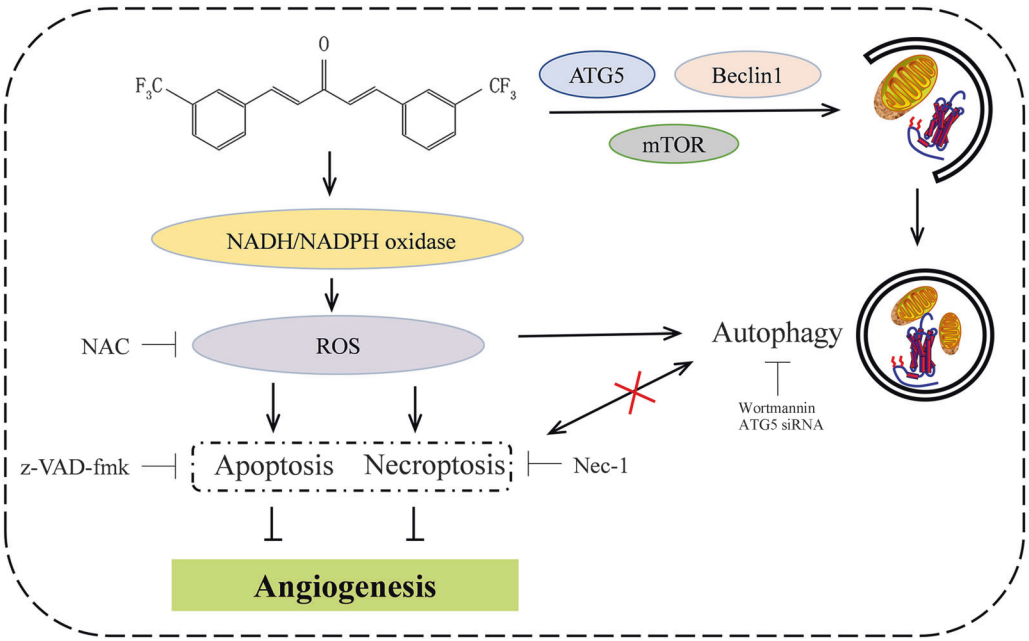

Fig. 9 Curcumin analog A2-mediated intracellular signaling that involves in its anti-angiogenesis effect. Black arrows, activation; black blocks, inhibition; cross, no interaction

endothelial cells are relatively more vulnerable to exogenous ROS-generating compounds. A further increase in ROS is likely to push ROS levels above the toxic threshold that these cells can bear, leading to cell death [32]. Data from flow cytometry showed that curcumin analog A2 enhanced ROS levels in HUVECs. Although ROS can be endogenously produced by several cellular sources, NADH/NADPH oxidase and mitochondria are believed to be the major sources of ROS in the endothelium [33]. We found that ROS in curcumin analog A2-treated HUVECs were mainly derived from NADH/NADPH oxidase. The ROS scavenger NAC nearly completely reversed the cytotoxic effects of curcumin analog A2 toward HUVECs, suggesting that curcumin analog A2-induced endothelial cell death was mediated by ROS. Moreover, ROS scavenging effectively reversed the antiangiogenic activity of curcumin analog A2 in vitro, ex vivo, and in vivo, confirming a vital role of ROS in the antiangiogenic effects of curcumin analog A2.

In conclusion, we first demonstrated that a monocarbonyl analog of curcumin, A2, exhibits potent antiangiogenic activity by inducing ROS-dependent endothelial cell death. Although curcumin analog A2 triggered endothelial cell autophagy, it appeared to not affect the cytotoxicity of curcumin analog A2 toward HUVECs, suggesting that the role of autophagy on endothelial cell fate triggered by different antiangiogenic agents needs to be examined. Curcumin analog A2 has the potential to be developed into a novel therapeutic agent targeting ROS for inducing endothelial cell death and treating angiogenesis-related diseases.

ACKNOWLEDGEMENTS

This work was supported by the National Natural Science Foundation of China (No. 31471296), the Foundation for Key Teacher by Henan University of Technology (No. 001170) and the Research Program for Science and Technology of Henan Province (No. 192102310148).

AUTHOR CONTRIBUTIONS

LZ designed the study; BL, LSC, BZ, LLZ, ZHL, and LZ performed the study; BL and LZ analyzed the data; LZ wrote the paper.

ADDITIONAL INFORMATION

The online version of this article (https://doi.org/10.1038/s41401-019-0224-x) contains supplementary material, which is available to authorized users.

Competing interests: The authors declare no competing interests.

REFERENCES

1. Potente M, Gerhardt H, Carmeliet P. Basic and therapeutic aspects of angiogenesis. Cell. 2011;146:873–87.
2. De Palma M, Biziato D, Petrova TV. Microenvironmental regulation of tumour angiogenesis. Nat Rev Cancer. 2017;17:457–74.
3. Hida K, Hida Y, Shindoh M. Understanding tumor endothelial cell abnormalities to develop ideal anti-angiogenic therapies. Cancer Sci. 2008;99:459–66.
4. Noble ME, Endicott JA, Johnson LN. Protein kinase inhibitors: insights into drug design from structure. Science. 2004;303:1800–5.
5. Rahmani AH, Alsahli MA, Aly SM, Khan MA, Aldebasi YH. Role of curcumin in disease prevention and treatment. Adv Biomed Res. 2018;7:38.
6. Shanmugam MK, Warrier S, Kumar AP, Sethi G, Arfuso F. Potential role of natural compounds as anti-angiogenic agents in cancer. Curr Vasc Pharmacol. 2017;15:503–19.
7. El-Azab M, Hishe H, Moustafa Y, El-Awady El-S. Anti-angiogenic effect of resveratrol or curcumin in Ehrlich ascites carcinoma-bearing mice. Eur J Pharmacol. 2011;652:7–14.
8. Gururaj AE, Belakavadi M, Venkatesh DA, Marmé D, Salimath BP. Molecular mechanisms of anti-angiogenic effect of curcumin. Biochem Biophys Res Commun. 2002;297:934–42.
9. Hewlings SJ, Kalman DS. Curcumin: A review of its' effects on human health. Foods . 2017;6:E92.
10. Shimazu K, Inoue M, Sugiyama S, Fukuda K, Yoshida T, Taguchi D, et al. Curcumin analog GOY078, overcomes resistance to tumor angiogenesis inhibitors. Cancer Sci. 2018;109:3285–93.
11. Sugiyama S, Yoshino Y, Kuriyama S, Inoue M, Komine K, Otsuka K, et al. A curcumin analog, GO-Y078, effectively inhibits angiogenesis through actin disorganization. Anticancer Agents Med Chem. 2016;16:633–47.
12. Sun L, Liu J, Lin SS, Shi WT, Zhu J, Liang G, et al. Potent anti-angiogenic activity of B19–a mono-carbonyl analogue of curcumin. Chin J Nat Med. 2014;12:8–14.
13. Zhao C, Liu Z, Liang G. Promising curcumin-based drug design: mono-carbonyl analogues of curcumin (MACs). Curr Pharm Des. 2013;19:2114–35.
14. Pan Z, Chen C, Zhou Y, Xu F, Xu Y. Synthesis and cytotoxic evaluation of monocarbonyl analogs of curcumin as potential anti-tumor agents. Drug Dev Res. 2016;77:43–9.

15. Pignanelli C, Ma D, Noel M, Ropat J, Mansour F, Curran C, et al. Selective targeting of cancer cells by oxidative vulnerabilities with novel curcumin analogs. Sci Rep. 2017;7:1105.
16. Song JX, Sun YR, Peluso I, Zeng Y, Yu X, Lu JH, et al. A novel curcumin analog binds to and activates TFEB in vitro and in vivo independent of MTOR inhibition. Autophagy. 2016;12:1372–89.
17. Jaffe EA, Nachman RL, Becker CG, Minick CR. Culture of human endothelial cells derived from umbilical veins. Identification by morphologic and immunologic criteria. J Clin Invest. 1973;52:2745–56.
18. Zhang L, Jing H, Cui L, Li H, Zhou B, Zhou G, et al. 3,4-Dimethoxystilbene, a resveratrol derivative with anti-angiogenic effect, induces both macroautophagy and apoptosis in endothelial cells. J Cell Biochem. 2013;114:697–707.
19. Zhang L, Wang X, Miao Y, Chen Z, Qiang P, Cui L, et al. Magnetic ferroferric oxide nanoparticles induce vascular endothelial cell dysfunction and inflammation by disturbing autophagy. J Hazard Mater. 2016;304:186–95.
20. Zhang L, Dai F, Cui L, Jing H, Fan P, Tan X, et al. Novel role for TRPC4 in regulation of macroautophagy by a small molecule in vascular endothelial cells. Biochim Biophys Acta. 2015;1853:377–87.
21. Patan S. Vasculogenesis and angiogenesis. Cancer Treat Res. 2004;117:3–32.
22. Klionsky DJ, Abdelmohsen K, Abe A, Abedin MJ, Abeliovich H, Acevedo Arozena A, et al. Guidelines for the use and interpretation of assays for monitoring autophagy (3rd edition). Autophagy. 2016;12:1–222.
23. Redza-Dutordoir M, Averill-Bates DA. Activation of apoptosis signalling pathways by reactive oxygen species. Biochim Biophys Acta. 2016;1863:2977–92.
24. Ramjiawan RR, Griffioen AW, Duda DG. Anti-angiogenesis for cancer revisited: Is there a role for combinations with immunotherapy? Angiogenesis. 2017; 20:185–204.
25. Risau W. Mechanisms of angiogenesis. Nature. 1997;s386:671–4.
26. Sakamaki K. Regulation of endothelial cell death and its role in angiogenesis and vascular regression. Curr Neurovasc Res. 2004;1:305–15.
27. Watson EC, Grant ZL, Coultas L. Endothelial cell apoptosis in angiogenesis and vessel regression. Cell Mol Life Sci. 2017;74:4387–403.
28. Jiang F. Autophagy in vascular endothelial cells. Clin Exp Pharmacol Physiol. 2016;43:1021–8.
29. Pathania AS, Wani ZA, Guru SK, Kumar S, Bhushan S, Korkaya H, et al. The anti-angiogenic and cytotoxic effects of the boswellic acid analog BA145 are potentiated by autophagy inhibitors. Mol Cancer. 2015;14:6.
30. Gurel-Gurevin E, Kiyan HT, Esener OBB, Aydinlik S, Uvez A, Ulukaya E, et al. Chloroquine used in combination with chemotherapy synergistically suppresses growth and angiogenesis in vitro and in vivo. Anticancer Res. 2018;38:4011–20.
31. Nishikawa T, Tsuno NH, Okaji Y, Sunami E, Shuno Y, Sasaki K, et al. The inhibition of autophagy potentiates anti-angiogenic effects of sulforaphane by inducing apoptosis. Angiogenesis. 2010;13:227–38.
32. Panieri E, Santoro MM. ROS signaling and redox biology in endothelial cells. Cell Mol Life Sci. 2015;72:3281–303.
33. Szewczyk A, Jarmuszkiewicz W, Koziel A, Sobieraj I, Nobik W, Lukasiak A, et al. Mitochondrial mechanisms of endothelial dysfunction. Pharmacol Rep. 2015;67:704–10.